Magnetic Resonance Imaging 57 (2019) 103–110

Contents lists available at ScienceDirect

Magnetic Resonance Imaging

journal homepage: www.elsevier.com/locate/mri

Original contribution

Visualizing and quantifying flow stasis in abdominal aortic aneurysms in men using 4D flow MRI☆

Magnus Ziegler[a,b,*], Martin Welander[a,c], Jonas Lantz[a,b], Marcus Lindenberger[a,d], Niclas Bjarnegård[a], Matts Karlsson[b,e], Tino Ebbers[a,b], Toste Länne[a,c], Petter Dyverfeldt[a,b]

[a] Division of Cardiovascular Medicine, Department of Medical and Health Sciences, Linköping University, Linköping, Sweden
[b] Center for Medical Image Science and Visualization (CMIV), Linköping University, Linköping, Sweden
[c] Department of Thoracic and Vascular Surgery, Linköping University, Linköping, Sweden
[d] Department of Cardiology, Linköping University, Linköping, Sweden
[e] Division of Applied Thermodynamics and Fluid Mechanics, Department of Management and Engineering, Linköping University, Linköping, Sweden

ARTICLE INFO

Keywords:
Abdominal aortic aneurysm
Hemodynamics
4D flow MRI
Flow stasis

ABSTRACT

Purpose: To examine methods for visualizing and quantifying flow stasis in abdominal aortic aneurysms (AAA) using 4D Flow MRI.

Methods: Three methods were investigated: conventional volumetric residence time (VRT), mean velocity analysis (MVA), and particle travel distance analysis (TDA). First, ideal 4D Flow MRI data was generated using numerical simulations and used as a platform to explore the effects of noise and background phase-offset errors, both of which are common 4D Flow MRI artifacts. Error-free results were compared to noise or offset affected results using linear regression. Subsequently, 4D Flow MRI data for thirteen (13) subjects with AAA was acquired and used to compare the stasis quantification methods against conventional flow visualization.

Results: VRT ($R^2 = 0.69$) was more sensitive to noise than MVA ($R^2 = 0.98$) and TDA ($R^2 = 0.99$) at typical non-contrast signal-to-noise ratio levels (SNR = 20). VRT ($R^2 = 0.14$) was more sensitive to background phase-offsets than MVA ($R^2 = 0.99$) and TDA ($R^2 = 0.96$) when considering a 95% effective background phase-offset correction. Qualitatively, TDA outperformed MVA (Wilcoxon $p < 0.005$, mean score improvement 1.6/5), and had good agreement (median score 4/5) with flow visualizations.

Conclusion: Flow stasis can be quantitatively assessed using 4D Flow MRI. While conventional residence time calculations fail due to error accumulation as a result of imperfect measured velocity fields, methods that do not require lengthy particle tracking perform better. MVA and TDA are less sensitive to measurement errors, and TDA generates results most similar to those obtained using conventional flow visualization.

1. Introduction

Abdominal Aortic Aneurysms (AAAs) are a common occurrence, found in roughly one in twenty men above 65 years of age, and their rupture presents an emergency [1]. Despite that, their growth patterns and rupture risk are poorly understood [2]. Currently, the diameter of the AAA is the most commonly used measurement for predicting the growth rate and rupture risk [2–4]. However, the diameter is not representative of the growth rate nor the rupture risk, and it fails to capture the complexities of aneurysmal flow which are likely to play a role [3,5]. Therefore, new metrics are needed to help detect high-risk aneurysms that do not meet current diameter-based treatment thresholds as well as to avoid interventions in patients with larger but low-risk aneurysms.

As a result of complex aortic or aneurysmal geometry, flow patterns such as recirculatory regions, vortices, and stagnation zones can develop. These complex local hemodynamics may affect the growth and rupture risk of AAAs. For example, regions with slow or recirculatory flow, i.e. stasis, provide opportunity for platelet adhesion and thrombus formation [6]. Intra-luminal thrombus (ILT) development increases the aneurysmal growth rate, and regions of the vessel wall can be weakened as they experience local hypoxia as a consequence of the ILT [7–10]. As flow stasis creates an environment favourable to thrombus initiation or growth, and therefore subsequent AAA growth, non-invasive medical

☆ Disclosures: None.

* Corresponding author at: University Hospital, Staircase A, floor 12, Department of Medical and Health Sciences, Division of Cardiovascular Medicine, SE-581 83 Linköping, Sweden.
E-mail address: magnus.ziegler@liu.se (M. Ziegler).

https://doi.org/10.1016/j.mri.2018.11.003
Received 16 July 2018; Received in revised form 10 November 2018; Accepted 11 November 2018

imaging methods capable of locating and quantifying these regions would be valuable in optimizing treatment. One such scenario could be an AAA with large areas of stasis that would be treated earlier, by for example an endovascular stent-graft, than otherwise indicated for an AAA with similar size but less flow stasis, in order to prevent further growth.

Various methods to identify and quantify regions of flow stasis have been proposed. For example, Lagrangian particle tracking approaches that account for where particles accumulate and how long they remain there [9,11–14], and the Eulerian concept of a virtual ink [9], have been used to study flow stasis in aneurysm models using computational fluid dynamics (CFD) data. While these methods are widely applied in investigations of noise-free CFD data, their application in medical imaging data can be expected to be hampered by the fact measured in-vivo data is subject to various artifacts. In particular, methods that require particle tracking through several cardiac cycles are especially vulnerable to the accumulation and propagation of error. Additionally, CFD simulations often require considerable computing resources, making their use in large cohort studies or clinical scenarios challenging. Therefore, new analysis methods may be required to investigate stasis in clinically acquired data.

Transesophageal echocardiographic (TEE) examinations have been used to investigate the thromboembolic risk generated by flow stasis in the left atrial appendage using measures such as the mean flow velocity or ejection fraction [15–17]. From these studies, threshold values for flow velocity and other hemodynamic parameters have been suggested to denote risk for thrombus growth or the potential for emboli as a result of flow stasis. Similar risk thresholds have not been presented for AAAs. Moreover, TEE cannot fully describe the intricate 3D flow patterns found in AAAs and therefore new methods to investigate flow stasis would be valuable.

Three-dimensional, three-directional, and time-resolved phase-contrast MRI (4D Flow MRI) offers direct, non-invasive measurement of cardiovascular hemodynamics [18]. Recently, the use of 4D Flow MRI for assessing flow stasis was demonstrated in the left atrium and its appendage by considering the normalized histogram of all velocities in concert with a velocity threshold sourced from ultrasound investigations [19–22]. However, flow stasis in the context of AAAs has not been explored using 4D Flow MRI.

Therefore, the aim of this study was to implement and evaluate methods for visualizing and quantifying regions of stasis inside AAAs using 4D Flow MRI. To this end, three different methods were compared: a volumetric residence time method as commonly used with CFD, a velocity thresholding method similar to those used with TEE and previous MRI investigations, and a new particle tracking method developed for use with 4D Flow MRI data.

2. Methods

2.1. Assessment of flow stasis

Three methods for quantitative determination of flow stasis were implemented in MATLAB (The Mathworks, Natick, MA).

The first method was a volumetric residence time (VRT) method where virtual blood particles are released from a volume of interest, and their movements are calculated forwards in time [11]. In this study, particles were released from the centre of each voxel within the AAA at the beginning of the cardiac cycle and traced forward through twenty cardiac cycles. Particle positions were calculated using a 4th order Runge-Kutta method with a time-step of 5 ms. The total amount of time that any individual particle resided within a given voxel was calculated. In this way, VRT indicates which regions of the aneurysm accumulate virtual particles and the cumulative length of time they resided there. To provide information on an aggregate scale, the total number of particles within the volume of interest throughout the simulation was recorded, alongside the time required to clear 50% of the particles from the volume [8,13].

The second method quantifies flow stasis through the analysis of a given voxel's temporal mean velocity and is referred to as mean velocity analysis (MVA). The threshold below which voxels were defined to be in stasis was 5 cm/s, defined after examining the mean velocity during diastole for a subset of five AAA subjects, and taking into account expected noise levels of 4D Flow velocity data based on the velocity encoding range and SNR-estimates [23]. The velocity threshold was estimated as $V_{stasis} = \frac{VENC}{SNR}$. This value also approximates the velocity below which 4D Flow MRI is less likely to measure accurately. Considering the acquisitions in this study, the velocity below which we are not likely to resolve accurately was estimated as between 3 cm/s and 5 cm/s ($\frac{120\ cm/s}{40}$, and $\frac{150\ cm/s}{30}$, respectively). The velocity threshold for stasis was selected the upper bound of this range. VENC values of 120 and 150 cm/s were considered as they were the most common VENC values, representing 11 of 13 subjects. SNR estimates of 40 and 30 represent a contrast-enhanced acquisition, and a high-quality non-contrast-enhanced acquisition, respectively. This method represents an Eulerian approach to stasis quantification, and can be considered the most direct approach for locating and quantifying areas of flow stasis. Moreover, MVA for stasis quantification is a good point of comparison for other methods because of its simplicity and its similarity to earlier studies that used TEE and MRI for assessing stasis.

The third method quantifies flow stasis through the analysis of the travel distance of virtual particles and is referred to as travel distance analysis (TDA). Particles were released into the velocity field after being seeded at the centre of each voxel within a volume of interest at each timeframe and traced forwards for one complete cardiac cycle. Particle positions were calculated using a 4th order Runge-Kutta method with a time-step of 5 ms. The total distance travelled for each particle was calculated for each emission. From this, the mean travel distance for a given particle released from every voxel was calculated. In this way, images with a contrast that corresponds to the mean travel distance are generated (see Fig. 1). Shorter mean travel distance implies a higher risk of stasis. In this study, voxels with mean travel distance below 25% of the maximum were defined as stasis, after considering the histograms of mean travel distances for a subset of five AAA subjects.

In addition to the quantitative approaches, aneurysmal flows were visually investigated using conventional flow visualizations within a commercially available software package (Ensight, CEI Inc., Apex, NC) to qualitatively assess and compare the levels of stasis in each aneurysm and identify potential regions of stasis (see Fig. 2, Supporting Video 1). Pathlines were created at a minimum of 1000 locations evenly distributed throughout the AAA, emitted on 0.1 s intervals through the cardiac cycle, and traced forward 0.2 s. Regions where pathlines appeared to stagnate or displayed consistently low velocities were considered to be in stasis.

2.2. Data acquisition and processing

MR images were acquired for 13 male subjects, recruited consecutively through a surveillance program for AAA in men, using a 3 T scanner (Philips Ingenia, Philips Healthcare, Best, the Netherlands) equipped with a 32-channel torso coil with 60 cm coverage. Inclusion criteria included: AAA diameter ≥ 3.5 cm from ultrasound examination, non-smokers, not diabetic, held a sinus rhythm, and no contra-indications for MRI. Subjects with previous cardiovascular events were excluded. The study was approved by the regional ethical review board, and all subjects gave written informed consent.

4D Flow velocity data was acquired with a free-breathing, respiratory navigator gated, retrospectively cardiac-gated sequence following administration of a Gadolinium based contrast agent (Magnevist, Bayer Schering Pharma AG). Scan parameters included: a sagittal-oblique slab (‘Candy Cane’ view) with 3D field of view

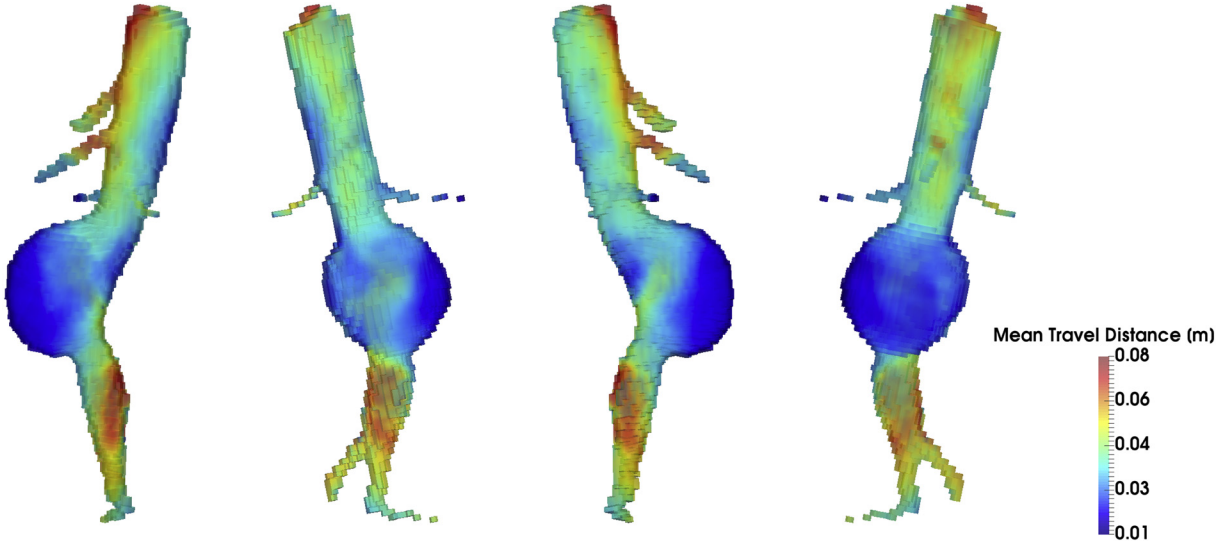

Fig. 1. Mean Travel Distance volume generated using the TDA method for one representative patient (AAA06). The mean travel distance represents the mean distance travelled by a particle in one cardiac cycle from a given spatial location. Shorter mean travel distance implies a higher risk of stasis.

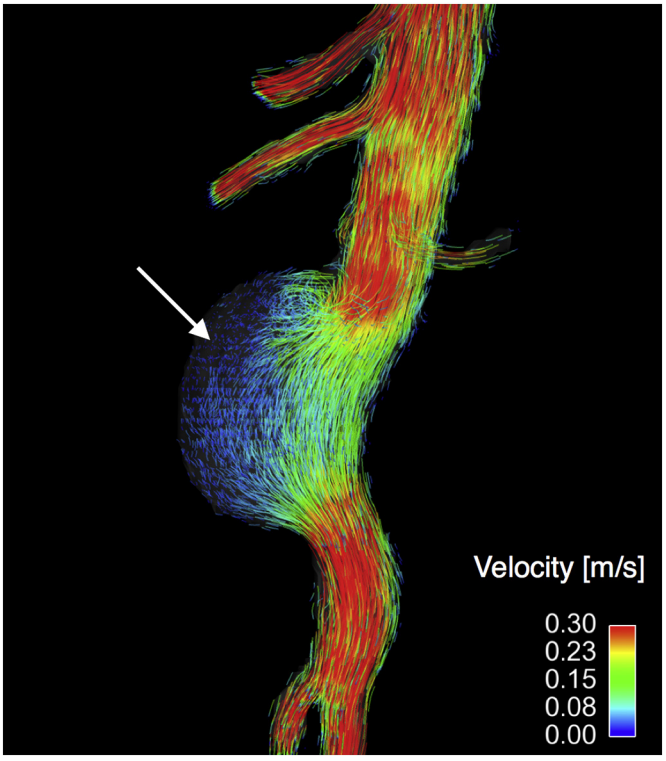

Fig. 2. Example pathline visualization per analysis protocol for a representative patient (AAA06) in late systole. Arrow indicates a region identified as stasis inside the aneurysm.

(FOV) = 480–560 × 480–560 × 70–105 mm^3 and matrix size = 192–224 × 192–224 × 28–42 set to cover the whole aorta from left ventricular outflow tract to iliac bifurcation, velocity encoding range (VENC) 100–180 cm/s (set based on the expected peak velocity in the descending aorta), flip angle 15°, echo time 2.5–3.1 ms, repetition time 4.4–5.0 ms, k-space segmentation factor 2, acquired temporal resolution 35–40 ms, and acquired spatial resolution 2.5 × 2.5 × 2.5 mm^3. SENSE parallel imaging was used, with a total acceleration factor of 4–4.8. Data was reconstructed to 40 timeframes. Total scan time including navigator efficiency was 10–15 min. 4D Flow datasets were corrected for concomitant gradient field effects on the scanner, while phase-wraps and background phase-offset errors were corrected offline. Background phase-offset errors were corrected using a weighted 4th order fit to static tissue [24].

Contrast-enhanced MR angiography (CE-MRA) volumes were acquired and used to segment the inner lumen of the aorta. AAA length was also estimated using the CE-MRA volume. Scan parameters included: a sagittal-oblique slab ('Candy Cane' view) set to cover the whole aorta from left ventricular outflow tract to iliac bifurcation, flip angle 30°, echo time 2 ms, repetition time 5.8 ms, parallel imaging (SENSE) factor 4, and spatial resolution 0.6 × 0.6 × 1.2 mm.

Balanced steady-state free procession (bSSFP) images were acquired and used to assess aneurysm and thrombus morphology. Scan parameters included: axial slab covering the abdominal aorta, flip angle 60°, echo time 1.5 ms, repetition time 3.1 ms, and spatial resolution 1.4 × 1.4 × 5 mm.

The aorta and aneurysm were segmented using an in-house semi-automatic region-growing algorithm on the CE-MRA images and subsequently down-sampled and registered to the 4D Flow volumes using a rigid transformation matrix. AAA length was estimated from the CE-MRA images using a straight-line distance tool. AAA morphology was visually determined by one observer (*M.Z*).

2.3. Impact of noise and background phase-offset errors

The sensitivity of the stasis quantification methods to noise and background phase-offset errors was analyzed by gradually degrading ideal numerical velocity data for one large saccular aneurysm (subject AAA06). The ideal numerical velocity data was obtained using computational fluid dynamics (CFD) by solving the Navier-Stokes equations using ANSYS CFX 17.0 (ANSYS Inc., Canonsburg, PA). The computational mesh was created with ANSYS ICEM 16.0 [25–27]. AAA geometry and the inlet flow profile used for boundary conditions were derived from the CE-MRA and 4D Flow MRI data, respectively. A zero relative pressure boundary condition was set at the distal outlet of the AAA, and arterial branches proximal to the AAA were given time-varying flow profiles from 4D Flow MRI data. Walls were rigid and obeyed the no-slip condition. The working fluid was incompressible with a density of 1060 kg/m^3, and dynamic viscosity of 3.5×10^{-3} Pa·s. Seven cardiac cycles were simulated, totaling six seconds, and exported on 20 ms intervals to mimic 4D Flow MRI sampling rates. The high resolution numerical velocity field was downsampled using a Gaussian kernel to mimic 4D Flow MRI spatial resolution.

Five levels of Gaussian noise were added to the ideal velocity field, corresponding to signal-to-noise ratio (SNR) levels of: 3, 5, 10, 20, and 40. An SNR of 20 represents a conservative estimate of the SNR for non-contrast enhanced 4D Flow MRI [23]. The effects of background phase-offsets were examined by adding the offset field derived from 4D Flow MRI for subject AAA06, which was 1.5 cm/s on average in each direction inside the aneurysm. The impact of the offsets was examined by progressively reducing the strength of the offsets, to simulate the corrections commonly performed on 4D Flow MRI data. Five levels of correction efficacy were examined, corresponding to reductions in the background phase-offsets of: 0% (i.e., no reduction), 50%, 75%, 90%, and 95%.

2.4. Statistical analysis

The effects of noise and background phase-offsets on the stasis assessment methods were examined by comparing the noise or offset corrupted results to the results obtained with the uncorrupted ideal velocity field using linear regression. The coefficient of determination (R^2) was reported for each regression, and regression models had their intercepts fixed to zero. A two-tailed *t*-test was used to determine whether or not the slopes of the regression lines were statistically different than zero.

To investigate the cumulative effects of noise and background phase-offset errors on long duration particle tracking, the particle washout profiles from noise or offset-corrupted data were compared to results from the ideal velocity data. The 50% clearance time was also used as an aggregate measure of the impact and used for comparison.

After excluding the VRT method from further analysis due to excessive sensitivity towards typical levels of artifacts seen in 4D Flow MRI velocity data, the agreement between the two remaining stasis quantification methods was quantitatively assessed by comparing the volume identified as stasis for each AAA. Qualitative agreement between MVA and TDA was also evaluated, by visually comparing the size and location of highlighted stasis regions. Finally, stasis regions identified using MVA and TDA were compared against the regions identified using conventional pathline flow visualizations. Qualitative assessments were performed by two observers (*M.Z.*, *P.D.*). In each comparison, agreement was scored from 0 to 4, where: 0 = No Agreement, 1 = Poor Agreement, 2 = Moderate Agreement, 3 = Good Agreement, and 4 = Excellent Agreement.

A two-tailed *t*-test was used to determine whether or not there was a statistically significant difference between the amount of stasis identified in each subject using TDA and MVA. The mean and standard deviation of the difference between the two methods was also reported.

The Wilcoxon signed-rank test was used to compare the results of visual agreement scoring between MVA and TDA methods, and to determine if there was a difference between the two observers. In addition to the Wilcoxon signed-rank test, a two-tailed *t*-test was used to determine which quantitative method was superior, with a superiority margin of 1.

A p-value < 0.05 was considered significant. Values are presented as mean ± standard deviation, unless otherwise noted.

3. Results

4D Flow MRI was successfully acquired for 13 subjects (age: 71 ± 3 years, Table 1) with infrarenal AAA. Subjects were 1.76 ± 0.04 m tall and weighed 87.5 ± 10.8 kg. Average BSA was 2.05 ± 0.13 m^2. Considering only the shape of the lumen, four subjects had saccular morphology, and nine had fusiform morphology. Segmentations for each subject can be seen in Supporting Fig. S1.

Noise strongly affected the VRT method (Table 2, Fig. 3). For example, there is substantial impact ($R^2 = 0.68$) at typical SNR of 20, though only a small difference in 50% clearance time. Noise affected the MVA method more than the TDA method when SNR is at or below the typical non-contrast SNR of 20 (Table 2). For example, at SNR = 20, the stasis volume identified by the MVA method was reduced by 29%, but there was only a 4% reduction using the TDA method.

The presence of background phase-offsets in the velocity field had a substantial impact on methods based on particle tracking (Table 3). Broadly, as the effectiveness of the background-offset correction is reduced, the correlation to offset-free results is reduced. For example, considering the velocity field with completely uncorrected background phase-offsets, no similarity to offset-free results was found for the VRT method ($R^2 = 0$), and the TDA method was similarly impacted ($R^2 = 0.08$). The TDA method performs better than the VRT method for each level of background-offsets considered. MVA, not being based on particle tracking, was more robust to offset errors than both the VRT and TDA methods. With respect to the VRT method, the time until 50% clearance shortened with larger offsets. Concerning the TDA method, there was no clear relationship between the indicated stasis volume and the severity of the offsets. The MVA method indicated progressively smaller stasis volumes with increased offset errors.

The aggregate impact of velocity field distortions to VRT results can be assessed using the particle washout profiles, shown in Fig. 3. The large deviations from the ideal case created by background phase-offsets can be seen, alongside the more moderate impact of noise.

The intra-aneurysmal stasis volumes identified by MVA and TDA are shown in Table 4, alongside the mean velocity and mean travel distance for each subject. MVA consistently deemed a larger proportion of the AAA to be in stasis than TDA (mean difference 20.7 ± 15.2%, $p < 0.05$). The mean travel distance volume and the corresponding stasis regions for each AAA are shown in Supporting Fig. S2, while the mean velocity volume and corresponding stasis regions from MVA are shown in Supporting Fig. S3.

Qualitative assessments of the agreement between conventional flow visualization and MVA or TDA are shown in Table 5. MVA had a median agreement score of 1 (Poor Agreement) while TDA had a median agreement score of 3 (Good Agreement), and the difference was significant ($p = 0.0039$). In the majority of cases, TDA was judged to have equal or better agreement to conventional flow visualization than MVA. TDA had a mean score advantage of 1.6 ± 0.47 (mean ± standard error) over MVA, surpassing the superiority margin of 1. In most cases, the agreement between TDA and MVA was poor (median score = 1). There was no statistically significant difference between the two reviewers (mean difference = 0, $p > 0.05$).

Fig. 4 shows example results from MVA and TDA for three subjects (AAA01, AAA06, and AAA08). As shown in Fig. 4 (A,B), AAA01 shows moderate agreement between stasis quantification methods when assessed visually. AAA06 (Fig. 4C,D) has stasis regions highlighted deep in the aneurysmal sac. AAA06 shows good agreement between MVA and TDA. AAA08 (Fig. 4E,F) is a subject where there was no agreement between stasis quantification methods. This subject, presenting with a fusiform lumen morphology, displayed similar mean travel distances throughout the AAA, and therefore, the TDA method did not identify any regions of stasis. However, as the velocity remained low, MVA deemed 37% of the AAA volume as stasis.

4. Discussion

This study examined different approaches for visualizing and quantifying aneurysmal flow stasis using 4D Flow MRI data. First, we examined the calculation of VRT and found that it is strongly affected by errors in the velocity field which complicate its use. Subsequently, we proposed and examined two additional methods, MVA and TDA, for quantifying flow stasis more suited to 4D Flow MRI data.

VRT, representing a group of methods commonly used with CFD data [8,9,11–13,30], was strongly affected by typical levels of noise and background phase-offsets present in 4D Flow MRI. For example, even at SNR 40, the performance of VRT was substantially impacted, yielding $R^2 = 0.74$, compared to $R^2 = 0.99$ for both MVA and TDA. Similarly,

Table 1
Subject demographics and AAA overview.

Subject	Age [years]	Height [m]	Weight [kg]	BSA [m^2]	AAA morphology	AAA lumen diameter [mm]	Estimated AAA length [mm]	AAA region lumen volume [ml]
AAA01	70	1.69	72	1.84	Saccular	48	90	84
AAA02	69	1.72	100	2.19	Fusiform	45	80	66
AAA03	71	1.76	69	1.84	Fusiform	38	65	49
AAA04	66	1.81	105	2.29	Saccular	56	120	152
AAA05	69	1.76	94	2.13	Fusiform	37	75	70
AAA06	70	1.84	85	2.08	Saccular	50	90	124
AAA07	75	1.72	77	1.92	Saccular	44	90	73
AAA08	70	1.76	100	2.20	Fusiform	40	95	85
AAA09	75	1.73	90	1.96	Fusiform	30	55	41
AAA10	76	1.74	80	1.96	Fusiform	30	60	42
AAA11	68	1.82	83	2.04	Fusiform	37	100	100
AAA12	75	1.70	96	2.13	Fusiform	44	100	85
AAA13	69	1.78	86	2.05	Fusiform	50	110	107

Table 2
Effects of signal noise on volumetric residence time (VRT), travel distance analysis (TDA), and mean velocity analysis (MVA) stasis quantification methods with respect to noise-free CFD results.

Noise level	Time to 50% clearance, VRT [s]	R^2, VRT	Stasis volume, TDA [ml]	R^2, TDA	Stasis volume, MVA [ml]	R^2, MVA
Noise free	1.14	1.0	11.88	1.00	11.73	1.00
SNR 40	1.13	0.74	11.71	0.99	10.80	0.99
SNR 20	1.12	0.69	11.45	0.98	8.33	0.99
SNR 10	1.09	0.57	10.90	0.94	1.49	0.93
SNR 5	1.06	0.40	9.92	0.86	0	0.49
SNR 3	1.00	0.31	7.54	0.69	0	0

Note: All regression slopes were significantly different than zero.

considering background phase-offsets, VRT fared the worst among the methods tested. The poor performance of this method is likely linked to the fact that particles need to be traced through several cardiac cycles, leading to excessive error accumulation. Accordingly, we believe that this class of methods has limited applicability when used with 4D Flow MRI data. This therefore led to the investigation of methods more suitable for use with 4D Flow MRI.

When comparing methods for stasis quantification more suitable for 4D Flow MRI data, the TDA method was found to be more robust to noise than the MVA method (Table 2), but the TDA method was in turn more affected by background phase-offset errors (Table 3). Previous studies have not investigated the effects of either SNR or background phase-offsets on quantifying flow stasis. With respect to the effects of noise on MVA, our results indicated that as SNR decreased, there were fewer voxels with mean velocity below the threshold value, causing indicated stasis levels to drop. Therefore, the threshold velocity value must be set with SNR in mind when using the MVA method. Both noise and background phase-offsets can be addressed by tailoring the 4D Flow MRI data acquisition and post-processing [18,33]. For example, the SNR can be increased by acquiring data post contrast injection, or by acquiring more data through the use of a lower parallel imaging factor, a larger field-of-view, or signal averaging. Background phase-offsets may be reduced by using appropriate gradient pre-emphasis or by applying corrections that exploit the fact that the measured velocity in static tissue should be zero [24,34,35].

The MVA method consistently identified a larger proportion of the AAA as being in stasis in comparison to the TDA method and the latter method appears to be more specific, often identifying little or no stasis in the AAA (Table 4). Qualitatively, the TDA method scored higher than the MVA method when compared to conventional flow visualizations (Table 5). In several cases, conventional flow visualizations suggested that the AAA had little or no stasis and TDA method mirrored this result, whereas MVA did not.

The quantification and visualization of aneurysmal flow stasis is not currently a routine investigation, in part because there is no widely-accepted definition of flow stasis, but also because simple approaches for analysis and visualization are not available. The TDA method proposed in this work is a straightforward approach for quantification and visualization of flow stasis that only requires a segmentation of the AAA and the 4D Flow MRI velocity fields as input. An automated approach for assessing flow stasis, such as the TDA method presented here, enables studies with larger patient cohorts as there is less operator input required compared to conventional flow inspection, and offers more

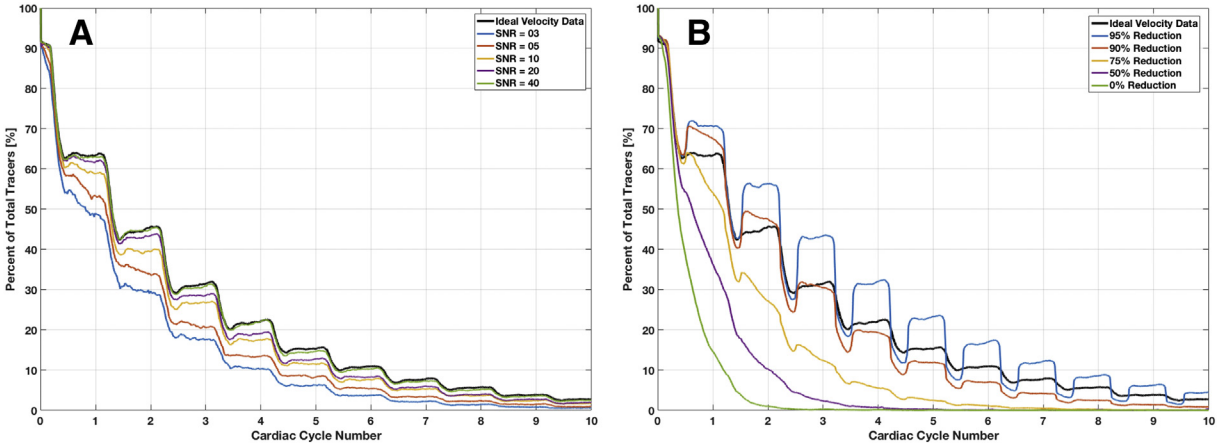

Fig. 3. Particle washout profiles generated using the numerically generated noise (A), and background phase-offset (B) 4D Flow data. Particle washout profiles show the proportion of particles in the volume of interest through time, and display the aggregate impact of velocity field distortions.

Table 3
Effects of background-phase offsets on volumetric residence time (VRT), travel distance analysis (TDA), and mean velocity analysis (MVA) stasis quantification methods with respect to offset-free results.

Background phase-offset correction [%]	Time to 50% clearance, VRT [s]	R^2, VRT	Stasis volume, TDA [ml]	R^2, TDA	Stasis volume, MVA [ml]	R^2, MVA
100% (i.e no offsets)	1.14	1.0	11.88	1.00	11.73	1.00
95%	1.14	0.14	9.93	0.96	11.47	0.99
90%	1.12	0.33	9.28	0.89	11.25	0.99
75%	1.05	0.32	9.78	0.60	10.31	0.98
50%	0.66	0.10	11.86	0.18	8.42	0.93
0%	0.37	0	11.98	0.08	4.22	0.71

Note: All regression slopes were significantly different than zero.

Table 4
Stasis quantification results from travel distance analysis and mean velocity analysis methods.

Subject	Mean travel distance [m]	Stasis volume TDA [%]*	Mean velocity [m/s]	Stasis volume MVA [%]*
AAA01	0.040	7%	0.079	20%
AAA02	0.050	4%	0.090	11%
AAA03	0.019	18%	0.074	21%
AAA04	0.054	0%	0.096	3%
AAA05	0.042	1%	0.086	12%
AAA06	0.035	13%	0.080	34%
AAA07	0.037	1%	0.062	41%
AAA08	0.043	0%	0.064	37%
AAA09	0.046	0%	0.065	17%
AAA10	0.060	0%	0.078	7%
AAA11	0.020	1%	0.068	26%
AAA12	0.030	0%	0.064	43%
AAA13	0.037	1%	0.067	43%

* Stasis volume normalized to AAA mask volume.

consistent results. These benefits would be realized in longitudinal studies of patients with AAA, where stasis could be tracked alongside ILT or AAA growth.

Previous investigations of flow stasis in AAAs have predominantly used CFD simulations and relied on metrics like the particle residence time [8,13,14,30]. These CFD-based studies have not sought to define thresholds to quantify total stasis volumes and instead focused on describing flow patterns. Considering the poor performance of the VRT method in this study, Lagrangian methods requiring particle tracing through several cycles, as commonly used with CFD data, are not advisable for use with 4D Flow MRI data. Previous 4D Flow MRI-based studies of flow stasis have examined flow velocities in the left atrium and classified voxels as being in stasis if their velocity is below a threshold value for the entire cardiac cycle [20,22]. The velocity-thresholding methodology represents an Eulerian approach for estimating flow stasis, similar to the MVA method described in this study. The application of the velocity threshold methodology in anatomical regions with substantial wall movement is conceptually challenging, even with the use of time-resolved segmentations. However, it is potentially suitable for scenarios with limited wall motion, such as AAA. The MVA method reported in the present study represents such a method.

This study has several limitations. The CFD simulation used to examine the effect of noise and background phase-offsets was based on a rigid wall model which may alter the near-wall hemodynamics. However, this effect is expected to be minor and not alter the results of this study, as the vessel wall in this area is relatively rigid. Another limitation is the use of different types of thresholds in the MVA and TDA methods and the approach used to determine the thresholds. Similar to previous studies, our implementation of the MVA method uses a fixed velocity threshold across the patient cohort and is therefore insensitive to patient specific flow conditions [20,22]. For example, given the range of aortic shapes and aneurysm locations, the expected (i.e. in healthy aortas) regional mean velocity varies, and therefore the velocity threshold for stasis may be too low or too high for a given patient. This may explain why MVA appeared to overestimate stasis, and highlights the difficulty in determining a suitable threshold value for cohort-wide use. The threshold used by the TDA method was similarly determined empirically, though it is relative to patient-specific, rather than cohort-wide, flow characteristics. Additionally, our study cohort consisted only of men, and it is possible that patient gender may need to be considered in the assessment and interpretation of flow stasis. Finally, while the flow stasis analyses used here are expected to indicate

Table 5
Qualitative agreement among stasis assessment methods.

Subject	Agreement: Mean Velocity Analysis vs. Travel Distance Analysis		Agreement: Travel Distance Analysis vs. Conventional Flow Analysis		Agreement: Mean Velocity Analysis vs. Conventional Flow Analysis	
	Reviewer 1	Reviewer 2	Reviewer 1	Reviewer 2	Reviewer 1	Reviewer 2
AAA01	2	3	3	3	2	2
AAA02	2	0	2	3	2	1
AAA03	2	1	1	3	1	1
AAA04	0	1	2	1	1	4
AAA05	1	1	1	3	1	1
AAA06	3	3	3	4	3	3
AAA07	1	0	2	2	1	1
AAA08	0	0	3	3	1	0
AAA09	0	0	3	2	1	1
AAA10	0	0	4	3	0	1
AAA11	1	0	3	3	1	1
AAA12	1	0	4	1	1	1
AAA13	1	0	4	4	1	2
Median (IQR)	1 (1)		3 (1)		1 (1)	

0 - No Agreement, 1 - Poor Agreement, 2 - Moderate Agreement, 3 - Good Agreement, 4 - Excellent Agreement.

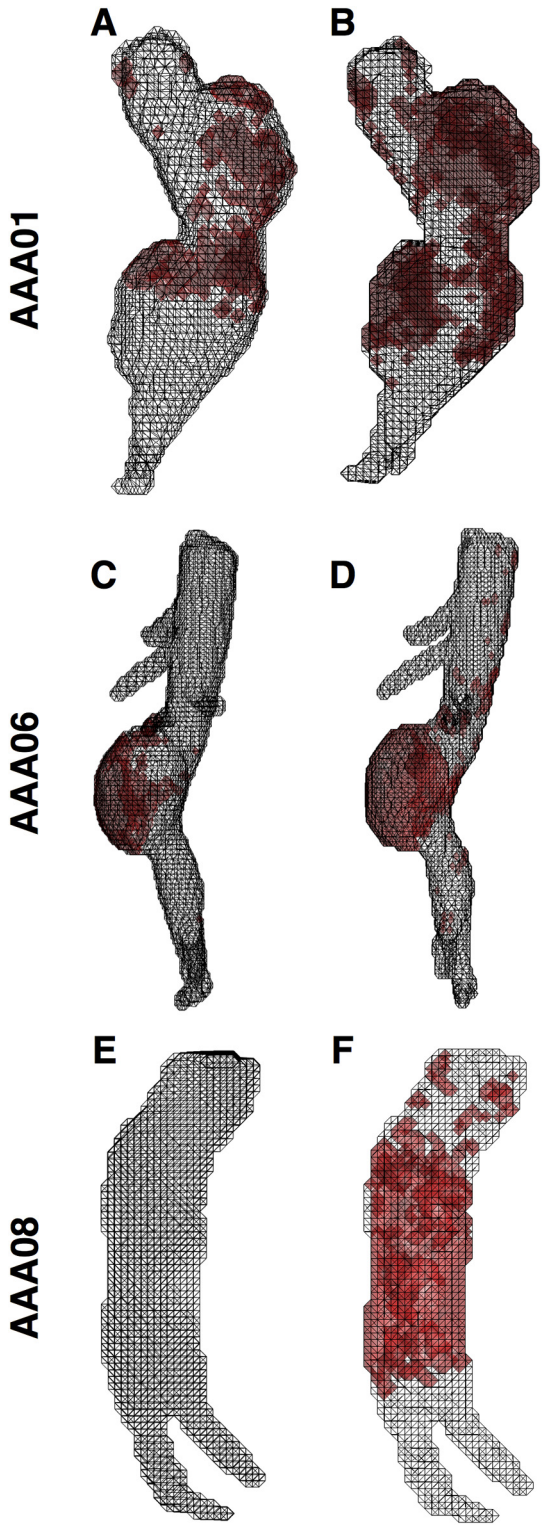

Fig. 4. Example delineations of regions with flow stasis for three patients (AAA01, AAA06, and AAA08) using both the travel distance analysis (A,C,E) and mean velocity analysis (B,D,F) methods. Regions highlighted in red are defined as being in stasis. (For interpretation of the references to colour in this figure legend, the reader is referred to the web version of this article.)

little or no stasis in subjects without aneurysms, we did not include such subjects in this study and can therefore only draw conclusions related to subjects with AAA.

In conclusion, this study assessed approaches for visualizing and quantifying flow stasis in AAAs using 4D Flow MRI. Computation of residence time, as commonly used with CFD data, was found to be unsuitable for use with 4D Flow MRI data due to excessive sensitivity to common measurement errors. The MVA and TDA methods were more robust to velocity field distortions and the latter method compared most favourably against conventional pathline visualizations. Imaging-based quantification of flow stasis may present another avenue for risk stratification or predicting intraluminal thrombus growth in AAA.

Supplementary data to this article can be found online at https://doi.org/10.1016/j.mri.2018.11.003.

Acknowledgements and grant support

The flow simulations were performed on resources provided by the Swedish National Infrastructure for Computing (SNIC) at the National Supercomputer Centre (NSC). Swedish Research Council, Medical Research Council of Southeast Sweden (FORSS), and the Swedish Heart and Lung Foundation. The authors thank Mats Fredrikson for his valuable advice concerning the statistical methods used in this study.

References

[1] Allen PI. Screening for abdominal aortic aneurysm. Biomed Pharmacother 1988;42:451–4. https://doi.org/10.1002/14651858.CD002945.pub2.www.cochranelibrary.com.
[2] Elefteriades JA. Thoracic aortic aneurysm: reading the enemy's playbook. Curr Probl Cardiol 2008;33:203–77. https://doi.org/10.1016/j.cpcardiol.2008.01.004.
[3] Dua MM, Dalman RL. Hemodynamic influences on abdominal aortic aneurysm disease: application of biomechanics to aneurysm pathophysiology. Vascul Pharmacol 2010;53:11–21. https://doi.org/10.1016/j.vph.2010.03.004.
[4] Hope MD, Wrenn SJ, Dyverfeldt P. Clinical applications of aortic 4D flow imaging. Curr Cardiovasc Imaging Rep 2013;6:128–39. https://doi.org/10.1007/s12410-012-9187-8.
[5] Lasheras JC. The biomechanics of arterial aneurysms. Annu Rev Fluid Mech 2007;39:293–319. https://doi.org/10.1146/annurev.fluid.39.050905.110128.
[6] Salsac A-V, Sparks SR, Lasheras JC. Hemodynamic changes occurring during the progressive enlargement of abdominal aortic aneurysms. Ann Vasc Surg 2004;18:14–21. https://doi.org/10.1007/s10016-003-0101-3.
[7] Vorp DA, Lee PC, Wang DHJDH, Makaroun MSM, Nemoto EM, Ogawa S, et al. Association of intraluminal thrombus in abdominal aortic aneurysm with local hypoxia and wall weakening. J Vasc Surg 2001;34:291–9. https://doi.org/10.1067/mva.2001.114813.
[8] Suh G-Y, Les AS, Tenforde AS, Shadden SC, Spilker RL, Yeung JJ, et al. Hemodynamic changes quantified in abdominal aortic aneurysms with increasing exercise intensity using mr exercise imaging and image-based computational fluid dynamics. Ann Biomed Eng 2011;39:2186–202. https://doi.org/10.1007/s10439-011-0313-6.
[9] Rayz VL, Boussel L, Ge L, Leach JR, Martin AJ, Lawton MT, et al. Flow residence time and regions of intraluminal thrombus deposition in intracranial aneurysms. Ann Biomed Eng 2010;38:3058–69. https://doi.org/10.1007/s10439-010-0065-8.
[10] Behr-Rasmussen C, Grøndal N, Bramsen MB, Thomsen MD, Lindholt JS. Mural thrombus and the progression of abdominal aortic aneurysms: a large population-based prospective cohort study. Eur J Vasc Endovasc Surg 2014;48:301–7. https://doi.org/10.1016/J.EJVS.2014.05.014.
[11] Kunov MJ, Steinman DA, Ethier CR. Particle volumetric residence time calculations in arterial geometries. J Biomech Eng 1996;118:158–64. https://doi.org/10.1115/1.2795954.
[12] Tambasco M, Steinman DA. On assessing the quality of particle tracking through computational fluid dynamic models. J Biomech Eng 2002;124:166. https://doi.org/10.1115/1.1449489.
[13] Suh G-Y, Les AS, Tenforde AS, Shadden SC, Spilker RL, Yeung JJ, et al. Quantification of particle residence time in abdominal aortic aneurysms using magnetic resonance imaging and computational fluid dynamics. Ann Biomed Eng 2011;39:864–83. https://doi.org/10.1007/s10439-010-0202-4.
[14] Arzani A, Suh G-Y, Dalman RL, Shadden SC. A longitudinal comparison of hemodynamics and intraluminal thrombus deposition in abdominal aortic aneurysms. Am J Physiol Heart Circ Physiol 2014;307:H1786–95. https://doi.org/10.1152/ajpheart.00461.2014.
[15] Handke M, Harloff A, Hetzel A, Olschewski M, Bode C, Geibel A. Left atrial appendage flow velocity as a quantitative surrogate parameter for thromboembolic risk: determinants and relationship to spontaneous echocontrast and thrombus formation–a transesophageal echocardiographic study in 500 patients with cerebral Isc. J Am Soc Echocardiogr 2005;18:1366–72. https://doi.org/10.1016/j.echo.2005.05.006.
[16] Goldman ME, Pearce LA, Hart RG, Zabalgoitia M, Asinger RW, Safford R, et al. Pathophysiologic correlates of thromboembolism in nonvalvular atrial fibrillation: I. Reduced flow velocity in the left atrial appendage (The stroke prevention in atrial fibrillation [SPAF-III] study). J Am Soc Echocardiogr 1999;vol. 12:1080–7. https://doi.org/10.1016/S0894-7317(99)70105-7.
[17] Pollick C, Taylor D. Assessment of left atrial appendage function by transesophageal

echocardiography. Implications for the development of thrombus. Circulation 1991;84:223–31.
[18] Dyverfeldt P, Bissell M, Barker AJ, Bolger AF, Carlhäll C-J, Ebbers T, et al. 4D flow cardiovascular magnetic resonance consensus statement. J Cardiovasc Magn Reson 2015;17:72. https://doi.org/10.1186/s12968-015-0174-5.
[19] Markl M, Carr M, Ng J, Lee DC, Jarvis K, Carr J, et al. Assessment of left and right atrial 3D hemodynamics in patients with atrial fibrillation: a 4D flow MRI study. Int J Cardiovasc Imaging 2016;32:807–15. https://doi.org/10.1007/s10554-015-0830-8.
[20] Markl M, Lee DC, Ng J, Carr M, Carr J, Goldberger JJ. Left atrial 4-dimensional flow magnetic resonance imaging: stasis and velocity mapping in patients with atrial fibrillation. Invest Radiol 2016;51:147–54. https://doi.org/10.1097/RLI.0000000000000219.
[21] Markl M, Foucar C, Carr ML, Lee DC, Ng J, Carr JC, et al. Left atrial and left atrial appendage 4D blood flow dynamics in atrial fibrillation. J Cardiovasc Magn Reson 2016;vol. 18:O90. https://doi.org/10.1186/1532-429X-18-S1-O90. (BioMed Central).
[22] Cibis M, Lindahl TL, Ebbers T, Karlsson LO, Carlhäll C-J. Left atrial 4D blood flow dynamics and hemostasis following electrical cardioversion of atrial fibrillation. Front Physiol 2017;8:1052. https://doi.org/10.3389/fphys.2017.01052.
[23] Bock J, Frydrychowicz A, Stalder AF, Bley TA, Burkhardt H, Hennig J, et al. 4D phase contrast MRI at 3 T: effect of standard and blood-pool contrast agents on SNR, PC-MRA, and blood flow visualization. Magn Reson Med 2010;63:330–8. https://doi.org/10.1002/mrm.22199.
[24] Ebbers T, Haraldsson H, Dyverfeldt P, Sigfridsson A, Warntjes MJB, Wigström L. Higher order weighted least-squares phase offset correction for improved accuracy in phase-contrast MRI. 16th meet. int. soc. magn. reson. med., Toronto. 2008. p. 1367.
[25] Ziegler M, Lantz J, Ebbers T, Dyverfeldt P. Assessment of turbulent flow effects on the vessel wall using four-dimensional flow MRI. Magn Reson Med 2016;00:1–10. https://doi.org/10.1002/mrm.26308.
[26] Lantz J, Renner J, Länne T, Karlsson M. Is aortic wall shear stress affected by aging? An image-based numerical study with two age groups. Med Eng Phys 2015;37:265–71. https://doi.org/10.1016/j.medengphy.2014.12.011.
[27] Lantz J, Gårdhagen R, Karlsson M. Quantifying turbulent wall shear stress in a subject specific human aorta using large eddy simulation. Med Eng Phys 2012;34:1139–48. https://doi.org/10.1016/j.medengphy.2011.12.002.
[30] Basciano C, Kleinstreuer C, Hyun S, Finol EA. A relation between near-wall particle-hemodynamics and onset of thrombus formation in abdominal aortic aneurysms. Ann Biomed Eng 2011;39:2010–26. https://doi.org/10.1007/s10439-011-0285-6.
[33] Schmitter S, Schnell S. 4D flow MRI. Quantif. biophys. parameters med. imaging Cham: Springer International Publishing; 2018. p. 187–212. https://doi.org/10.1007/978-3-319-65924-4_9.
[34] Walker PG, Cranney GB, Scheidegger MB, Waseleski G, Pohost GM, Yoganathan AP. Semiautomated method for noise reduction and background phase error correction in MR phase velocity data. J Magn Reson Imaging 1993;3:521–30. https://doi.org/10.1002/jmri.1880030315.
[35] Busch J, Vannesjo SJ, Barmet C, Pruessmann KP, Kozerke S. Analysis of temperature dependence of background phase errors in phase-contrast cardiovascular magnetic resonance. J Cardiovasc Magn Reson 2014;16:97. https://doi.org/10.1186/s12968-014-0097-6.